Equine Veterinary Journal

Equine Veterinary Journal ISSN 0425-1644
DOI: 10.1111/evj.12127

Experimental and Basic Research Studies

Three dimensional, radiosteriometric analysis (RSA) of equine stifle kinematics and articular surface contact: A cadaveric study

S. E. HALLEY, M. J. BEY†, J. A. HALADIK†, M. LAVAGNINO and S. P. ARNOCZKY*

Laboratory for Comparative Orthopaedic Research, Michigan State University, USA
†Bone and Joint Center, Henry Ford Hospital, Michigan, USA.

*Correspondence email: arnoczky@cvm.msu.edu; Received: 07.02.13; Accepted: 20.06.13

Summary

Reasons for performing study: Studies examining the effect of stifle joint angle on tibial rotation, adduction–abduction angle and articular contact area are lacking.
Objectives: To test the hypothesis that tibial rotation, adduction–abduction angle and articular contact area change with stifle joint angle.
Study design: Descriptive study of normal kinematics and articular contact patterns of the equine stifle through the functional range of motion using 3 dimensional (3D) radiosteriometric analysis (RSA) and equine cadaver stifles.
Methods: Multiple, radiopaque markers were embedded in the distal femur and proximal tibia and sequential, biplanar x-rays captured as the stifle was passively extended from 110° to full extension. Computer-programmed RSA was used to determine changes in abduction–adduction and internal–external rotation angles of the tibia during stifle extension as well as articular contact patterns (total area and areas of high contact) through the range of motion.
Results: The tibia rotated externally ($P<0.001$) as the stifle was extended. Tibial abduction occurred from 110–135° of extension ($P<0.001$) and tibial adduction occurred from 135° through full extension ($P = 0.009$). The centre of joint contact moved cranially on both tibial condyles during extension with the lateral moving a greater distance than the medial ($P = 0.003$). Articular contact area decreased ($P = 0.001$) in the medial compartment but not in the lateral compartment ($P = 0.285$) as the stifle was extended. The area of highest joint contact increased on the lateral tibial condyle ($P<0.001$) with extension but decreased ($P = 0.001$) on the medial tibial condyle.
Conclusions: Significant changes occur in tibial rotation, adduction–abduction angle and articular contact area of the equine stifle through the functional range of motion. Understanding the normal kinematics of the equine stifle and the relationship between joint positions and articular contact areas may provide important insight into the aetiology and location of common stifle joint pathologies (articular cartilage and meniscal lesions).

Keywords: horse; stifle; rotation; abduction-adduction; joint contact; 3D

Introduction

Stifle joint injuries (i.e. cartilage, menisci, ligaments) are becoming increasingly recognised in the equine [1–8]. While some of these injuries are likely related to acute overloading of the static stabilisers of the joint (e.g. damage to the cruciate and collateral ligaments), other conditions such as degenerative lesions of the menisci and cartilage may be related to alterations in the normal kinematics of the stifle [2,5–7,9]. The kinematic movement of a joint through the functional range of motion and the resulting mechanical loading environment is known to significantly influence the health and well-being of normal joints as well as the regeneration and healing of injured joint structures [10]. Changes in normal femoral–tibial joint kinematics have been shown to result in alterations in articular contact patterns and pressures which, in turn, can lead to pathological changes in the weightbearing structures (e.g. menisci, articular cartilage) [2,9–15]. Indeed, abnormal femoral–tibial joint kinematics have been implicated in a variety of joint pathologies in several species [2,11,12,16–22]. In addition, injuries which result from acute trauma or through the accumulation of microtraumatic events, such as meniscal tears, osteochondral lesions and/or ligament tears have also been shown to alter the normal kinematics of the stifle [6–8,18].

Previous studies of equine stifle kinematics have utilised a variety of methodologies including single-plane cinematography, electrogoniometry and optoelectronics [23–28]. However, these studies were mainly limited to identifying changes in joint angles in the sagittal plane during the gait cycle and did not address rotational or abduction–adduction changes through the range of motion [29]. Similarly, studies on equine articular contact have been limited to static analysis of joint motion using radiographs or electronic pressure sensors [2,30]. While such studies have provided important information, the ability to characterise both joint kinematics as well as articular surface contact patterns in 3 dimensions during dynamic movement of the stifle joint could significantly improve our understanding of the relationship between stifle joint anatomy, skeletal kinematics and the distribution of joint contact forces.

Studies in man and canines have utilised 3 dimensional (3D) radiosteriometric analysis (RSA) to identify joint kinematics as well as joint contact patterns during dynamic motion [21,31–35]. Radiosteriometric analysis utilises a collection of biplanar radiographic images to track the 3D positions of radiopaque markers within the distal femur and proximal tibia [31,32,36]. This information is combined with computed tomographic images to create a 3D model from which kinematic data can be calculated and joint contact patterns can be estimated [32–34,36]. Understanding the normal kinematics of the equine stifle and the relationship between joint positions and articular contact areas may provide important insight into the aetiology and location of common stifle joint pathologies (articular cartilage and meniscal lesions). Therefore, the purpose of this study was to describe the normal kinematics and estimated articular contact patterns of equine cadaver stifles through the functional range of motion using RSA. We hypothesise that normal equine stifles will demonstrate a consistent pattern of tibial rotation and abduction–adduction through the functional range of motion. We also hypothesise that articular surface contact patterns will change as a function of femoral–tibial angle.

Materials and methods

Specimen preparation

Stifles (n = 5) with no evidence of joint pathology were harvested from adult horses of varying breeds between the ages of 7 and 27 years subjected to euthanasia for unrelated causes. The distal third of the femur and the proximal third of the tibia were removed and the specimens were dissected free of their soft tissues leaving only the cruciate and collateral ligaments as well as the menisci and their associated meniscal ligaments intact. Specimens were wrapped in saline moistened towels and frozen at -20°C until testing. At the time of testing, 2 mm diameter, radiopaque, stainless steel reference beads were placed in a random pattern within the distal femur (n = 6 beads) and proximal tibia (n = 6 beads) of each stifle with

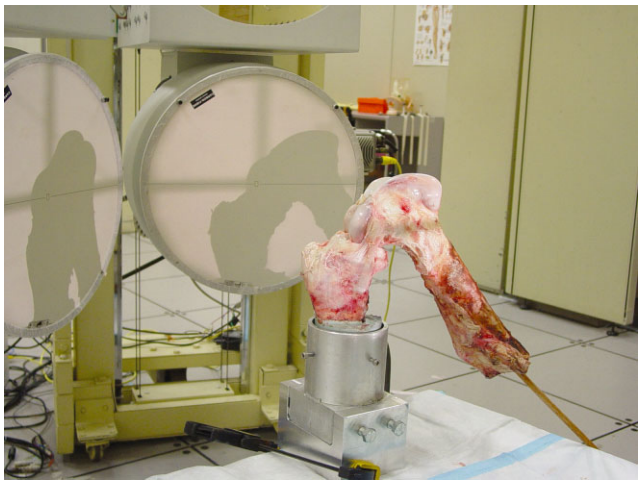

Fig 1: Photograph of the biplanar imaging set-up used in the current study. The equine tibia was secured in a custom-made aluminium fixture and the stifle extended while biplanar radiographic images were captured at 120 Hz.

the goal of maximising intermarker spacing and avoiding marker overlap in the radiographic views [37]. The tibia was then secured in a custom-made aluminium fixture, to maintain the limb in an upright orientation and positioned in the biplanar imaging apparatus (Fig 1).

Imaging protocol

The biplanar imaging set-up consisted of two 100 kW pulsed x-ray generators (CPX 3100CV)[a] and two 40 cm image intensifiers (AI5765HVP)[b] linked to high-speed video cameras (Phantom 9.1)[c] and anchored to a metal support. Prior to testing the stifle was taken through 3 full ranges of motion. Because previous RSA studies of *in vivo* running have demonstrated an across trial variability of less than 1° within subjects [32,34], a single trial was captured for each specimen.

The x-ray generators were set in pulse mode and images acquired at 120 Hz as the stifle was passively extended without any applied force in the medial or lateral directions from a femoral–tibial angle of 110° to full extension (as limited by condylar geometry and ligamentous constraints). This range of motion includes the stifle flexion angles documented for the weightbearing segment of the gait cycle at the walk, trot and gallop [22,28,29]. As previously described [37], custom software was used to determine the 3D position of each radiopaque marker from the biplanar radiographic images to an accuracy of within ± 0.1 mm. Subject-specific local anatomical coordinate systems were created for both the femur and tibia. The origin of the femoral coordinate system was defined as the halfway point between the centres of the medial and lateral condyle in the medial–lateral direction (X axis) and the halfway point between the most cranial point on the femur and the X axis (Y axis) so as to have the origin and the axes aligned with the femoral shaft. The origin of the tibial coordinate system was defined, as in previous studies, to be the 3D point located halfway between the most medial and lateral aspects of the tibial plateau [37,38]. Rotations of the tibia relative to the femur were defined with respect to the bone-fixed coordinate systems, and calculated using body-fixed axes in the order flexion–extension, adduction–abduction and internal–external rotation [38,39]. Neutral rotations (zero values) were defined as the position where the tibial and femoral coordinate systems were aligned. Positional changes of the radiopaque markers were used to calculate the rotational (internal/external) motion as well as abduction/adduction of the tibia relative to the femur through the range of motion for each stifle. For this study, degrees of extension were measured as the femoral-tibial angle. Computed tomography (CT) scans of each stifle were acquired using an in plane resolution of 0.47 mm and a slice thickness of 0.625 mm (GE Brightspeed 16 slice scanner)[d]. The CT images were reconstructed into a 3D model (Mimics)[e] and combined with the radiographic joint motion in a computer programme in order to create a 3D virtual model of each stifle [33].

Articular contact area

As noted above, the coupling of the biplanar radiographic images with the CT slices produced accurate models of the bone structures of the femur and tibia for each stifle specimen. However, since articular cartilage is radiolucent, to estimate articular surface contact patterns (total area and area of highest contact) it was necessary to assume an overall average cartilage thickness. Based on a previous publication [40], average thickness of equine articular cartilage on the femoral and tibial condyles was estimated to be approximately 2.2 mm. Thus, articular surface contact was estimated to occur when the radiographic gap between the subchondral surface of the tibia and femur was 4.5 mm or less. Joint contact patterns were estimated for each stifle by combining the joint motion measured from the biplanar radiographic images with the CT-based bone models. Specifically, the estimated joint contact centre was determined by calculating the minimum distance between the femur and tibia bone model surfaces at each point on the tibia and then determining the centroid of this distance map. The estimated contact centre was expressed relative to the tibia and the process repeated for all frames of every trial. These calculations resulted in a contact path, e.g. a time series of estimated joint contact centre data, expressed in terms of cranial–caudal and medial–lateral movement. The analysed bone surface area is shown in colour with beige corresponding to areas deemed not in contact and relative increases in the proximity of the bony condyles, and thus the predicted magnitude of joint contact, were depicted as changing colour patterns ranging from low contact (blue) to high contact (red) (Fig 2).

Two outcome measures were determined from the estimated joint contact data: total estimated contact area and high estimated contact area. Total estimated contact area, defined as the total area of estimated joint contact, was standardised by dividing the total estimated contact area at 5° increments of extension by the initial total estimated contact area at 110° of extension. The area of highest estimated contact (red) was standardised by dividing the high estimated contact area by the total estimated contact area at the corresponding angle of extension. The total estimated contact area and high estimated contact areas were

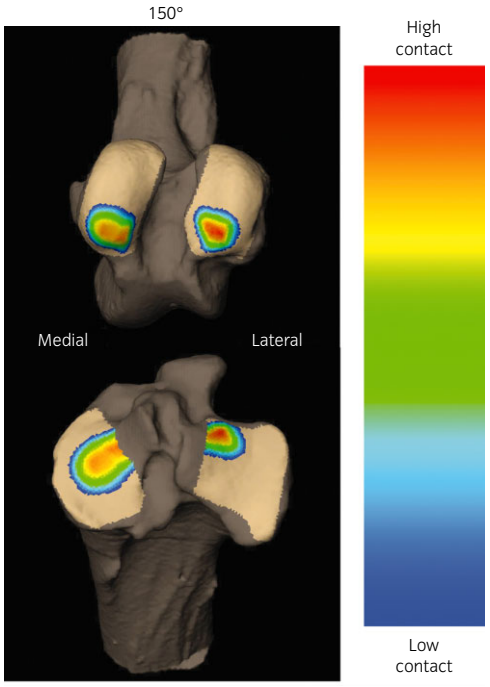

Fig 2: An example of computer generated 3 dimensional images illustrating the predicted articular contact patterns on the femoral and tibial condyles of one stifle at a joint angle of 150°. The colour patterns depict the relative degree of estimated cartilage contact from low (blue) to high (red). The beige colour represents areas of no cartilage contact.

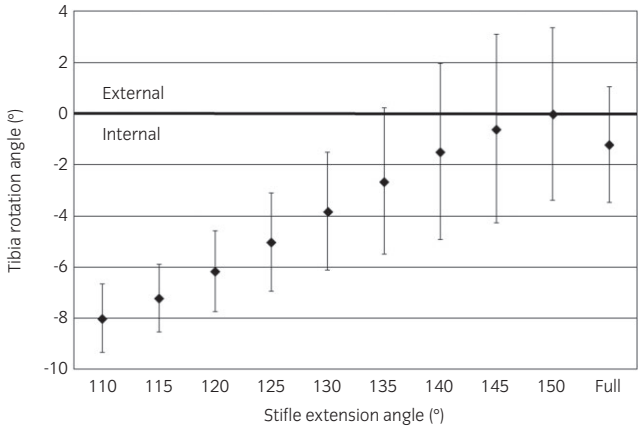

Fig 3: Graph illustrating the degrees of tibial rotation (mean ± s.d.) at corresponding femoral tibial angles from all 5 stifles. A significant (P<0.001) change in tibial rotation occurs over the range of motion.

standardised to each limb to eliminate limb to limb variability and to better demonstrate the relative changes in estimated articular contact area with degrees of extension of all horse stifles.

Data analysis

The results are based on one trial per stifle and the data represent the mean and standard deviation (mean ± s.d.) of the specific outcome metric from all 5 stifles. Rotation and abduction–adductions angles, as well as contact area data, were analysed using a repeated measures ANOVA to determine statistically significant changes over the flexion/extension angle range. The distances the estimated centre of articular contact moved between the lateral and medial joint compartments during the range of motion were compared using a paired *t* test.

Results

Full extension

The maximum angle of full passive extension ranged between horse limbs from 150 to 161° with mean ± s.d. of 156.4 ± 4.2.

Tibial rotation

All stifles demonstrated significant external rotation (P<0.001) of the tibia as the joint was extended from 110° through full extension (Fig 3).

Abduction–adduction

The tibias demonstrated a significant amount of abduction (P<0.001) as the stifles were extended from 110° to 135° (Fig 4). The tibia remained abducted until 140° of extension when it began to adduct through full extension (P = 0.009).

Articular contact area

The estimated centre of articular contact on the medial tibial plateau followed a caudal–medial to cranial–lateral path as the stifle was extended while the estimated centre of articular contact on the lateral tibia condyle followed a predominantly caudal to cranial path on the lateral condyle (Fig 5). The estimated centre of articular contact moved caudal to cranially significantly (P = 0.003) more on the lateral tibial condyle (16.3 ± 5.0 mm; mean ± s.d.) than on the medial tibial condyle (8.5 ± 3.0 mm). A similar finding has been reported in knees in human patients [41,42].

Standardised estimated contact area of the medial compartment decreases between 110° and full extension (100% to 81.3 ± 10.6%) (P<0.001). In the lateral compartment, overall estimated contact area remained unchanged throughout the range of motion (100% to 90.8 ± 18.6%) (P = 0.285).

The medial compartment of the stifle exhibited the greatest area of estimated high articular contact at 110° of extension (21.0 ± 13.6%). This area of estimated high articular contact decreased significantly between 110° and full extension reaching its nadir at 135° (5.0 ± 6.9%) (P = 0.001). The lateral compartment of the stifle demonstrated an initial negligible estimated high articular contact at 110° (0.9 ± 2.1%), but it significantly (P<0.001) increased over flexion angle until full extension (30.9 ± 10.8%).

Discussion

Abnormal femoral–tibial joint kinematics have been implicated in a variety of joint pathologies in several species [2,11,12,16–22]. Alterations in tibial rotation and articular surface contact patterns have been shown to play a significant role in the aetiology of meniscal and cartilage injuries [21,43–47]. However, to date, kinematic studies of the equine stifle have largely been limited to identifying changes in joint angles during the gait cycle and data regarding tibial rotation, tibial abduction–adduction angles and femoral–tibial joint contact patterns have been lacking [27–29]. The use of 3D radiosteriometric analysis allows documentation of joint motions (flexion–extension, axial rotation and abduction–adduction) around the 3 orthogonal axes of the stifle as well as a mechanism by which to estimate articular surface contact area and intensity through the range of motion.

The results of the current study demonstrate that extension of the equine stifle was accompanied by axial rotation of the tibia. Initially, with the stifle in flexion, the tibia was internally rotated approximately 8°. During extension the tibia rotated externally returning to its neutral (0° of rotation) position at 150° of extension. Rotation of the tibia relative to the femur during flexion and extension has been described in a variety of species including the canine, ovine, equine and human knee [11–13,20,30,48–50]. The rotation of the tibia occurs around a longitudinal axis and is governed by both the (femoral) condylar geometry and ligamentous constraints [11–13,49,51]. In flexion, the lateral collateral ligament becomes lax allowing the articular contact surface of the lateral femoral condyle to move more caudally on the tibia than the medial femoral condyle resulting in an internal rotation of the tibia [11–13,49,51]. As the stifle is extended and the lateral collateral ligament tightens, the articular contact surface of the lateral femoral condyles moves cranially on the tibia resulting in an external rotation of the tibia [49,52].

At 110° degrees of stifle flexion there was a slight, albeit significant, adduction of the tibia while extension of the stifle produced significant abduction of the tibia. A similar finding has been demonstrated in both man and canines [21,32,49,51] and is likely related to the aforementioned relaxation of the lateral collateral ligament during flexion of the stifle.

The joint contact patterns demonstrated in the current study were found to change with varying degrees of stifle joint extension. The centre of joint contact in each compartment moved cranially during extension

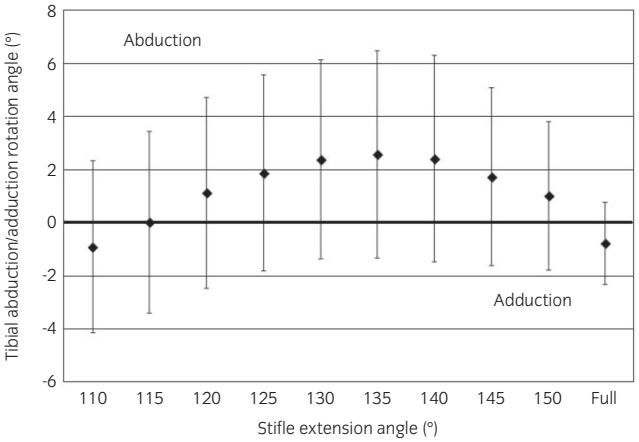

Fig 4: Graph illustrating tibial abduction and adduction angles (mean ± s.d.) at corresponding femoral tibial angles from all 5 stifles. Significant changes in the tibial abduction and adduction rotation angle occur over the 110–135° range (P<0.001) as well as between 140° and full extension (P = 0.009).

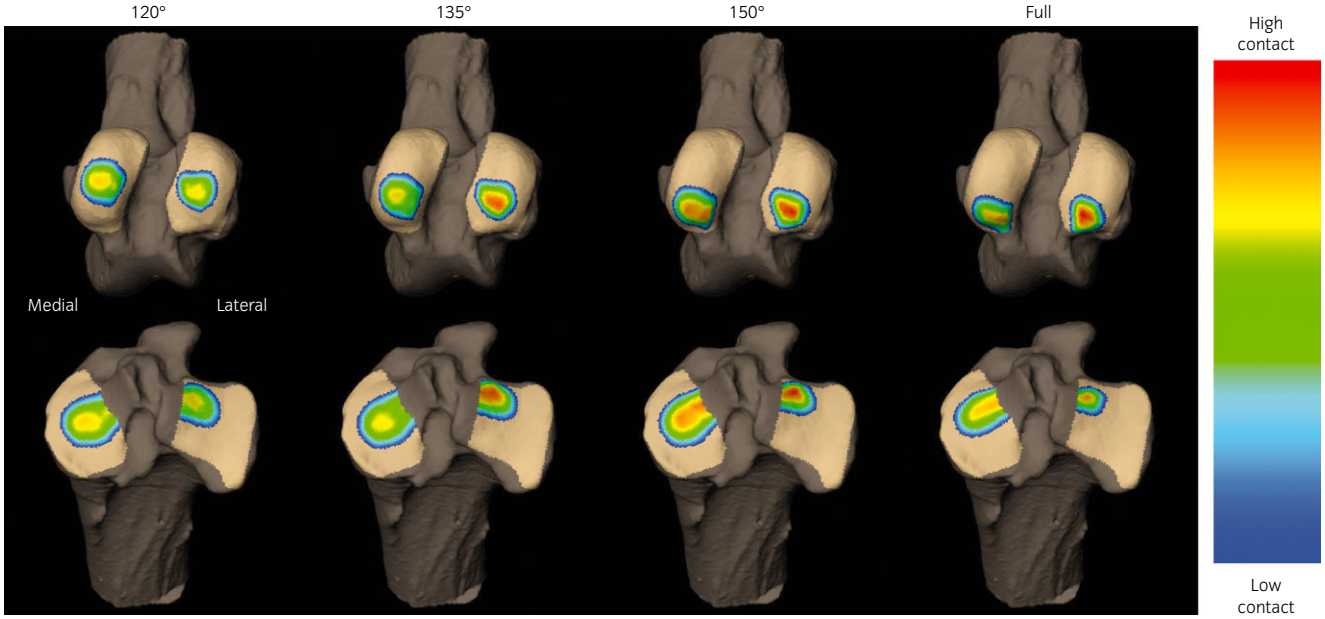

Fig 5: Images illustrating estimated articular contact patterns on both the femur and tibia at the indicated femoral–tibial angles from one representative stifle. The colour patterns depict the relative degree of estimated cartilage contact from low (blue) to high (red), while beige represents areas of no estimated cartilage contact.

with the centre of joint contact moving a significantly greater distance in the lateral compartment than the medial. A similar finding has been reported in an *in vivo* study in man using RSA [31] and an *in vivo* study using radio-opaque markers [41]. This motion has also been inferred from an *in vitro* radiographic study in the equine and was accompanied by a cranial translocation of the menisci during stifle extension and a caudal translocation of the menisci during flexion [22]. The greater movement of the centre of contact in the lateral compartment of the stifle appears to be associated with the aforementioned rotation of the tibia.

As noted previously, the joint contact patterns produced as a result of the RSA analysis are based on relative gap distance measurements between the subchondral surfaces of the femur and tibia. Therefore, these estimated contact patterns reflect actual cartilage to cartilage contact in regions of the joint not covered by the menisci. Indeed, the relative shape and movement of the total area of articular surface contact on both the medial and lateral tibial condyle demonstrated in the current study corresponds to the change in meniscal shape (and the shape of the area of articular cartilage not covered by the meniscus) demonstrated in previous studies [2,22]. In addition, the decrease in total articular contact area seen in both the lateral and medial compartments at terminal extension correlated with a previous *in vitro* study that demonstrated a significant decrease in articular contact area at a femoral tibia angle of 160° using electronic pressure sensors [2].

A previous study demonstrated considerable variability in compressive properties of osteochondral plugs harvested from various locations on the distal femur of healthy adult horses [53]. The investigators found that the aggregate moduli were highest in the medial femoral condyle and axial aspects of the lateral femoral condyle compared with the femoral trochlea [53]. In addition, they noted that bone strength and compressive modulus was highest in the central region of the medial femoral condyle [53]. Their results showed a 'bull's eye' pattern of increasing bone property values that was centred on the middle, nonmeniscus covered portions of the femoral condyle [53]. This pattern is similar to that of the relative articular contact areas demonstrated in the current study. Indeed, the locations of increased mechanical properties reported coincide with the areas of high articular contact intensity demonstrated by RSA. The increase in bone strength and compressive modulus at these condylar locations may possibly reflect an adaptive response to increased loading at these sites [54].

While it is tempting to try and correlate the areas of high articular contact demonstrated in this study with common locations of cartilage pathology, this approach would likely be too simplistic. The angle of the stifle joint during foot strike, magnitude of the applied joint load and ability of muscle forces to dissipate this load can all contribute with the mechanical environment experienced by the cartilage at impact. Additional studies are needed to determine how stifle kinematics and articular contact patterns are affected by alterations to the ligamentous constraints (e.g. too tight or too lax), alterations in gait patterns (e.g. loading at extremes of extension and/or flexion) and/or variations in the applied axis of loading. Such investigations may help identify the kinematic changes that could place the various components of the stifle (e.g. articular cartilage, ligaments, menisci) at risk of injury. In addition, because articular cartilage regeneration and healing is biologically dependent on the mechanical loading environment [10], minimising stifle motions that might overload areas of cartilage repair could be beneficial to cartilage repair and regeneration in the equine stifle joint. Therefore, the results of the current study could be used to identify ranges of motion that limit loading on various areas of both the femur and tibia.

A potential limitation of the current study was the absence of muscular forces in the test system. However, because rotation and abduction–adduction of the tibia are predominantly governed by the condylar geometry and ligamentous constraints of the femoral tibial joint [11,49,51] and not muscle forces, it was felt that the results of the current study provide a valid representation of these movements through the range of motion studied. Indeed, previous studies have shown excellent agreement between tibial rotation angles and femoral tibial angles between *in vitro* passive movement (no muscle loads) in cadaver knees [55] and *in vivo* running (active muscle loading) [32].

The inability to place a relevant load on the stifle joint throughout the range of motion was another potential limitation of the current study. While the absence of joint load likely did not affect the rotational or valgus–varus results for the aforementioned reasons, there was concern that the articular contact patterns would not be represented of what occurs in a loaded joint. A recent *in vitro* cadaveric study measured contact patterns in the medial compartment of the equine stifle using electronic pressure sensors [2]. In this study, equine stifles were statically loaded to 1800N at various degrees of flexion and the joint contact patterns recorded [2]. The location and area of high contact reported in that study were similar to those seen for the medial compartment of the stifle in the current investigation. This would suggest that although joint surface contact was not directly measured, the subchondral surface gap distance methodology employed in the 3D RSA [31,33], provided a

comparable representation of the articular surface contact patterns seen in the statically loaded test system [2].

Finally, while only one flexion to extension cycle was analysed from each specimen, previous RSA studies of *in vivo* running have demonstrated an across trial variability of less than 1° within subjects [32,34].

The results of the current study provide new information regarding the normal kinematics of the equine stifle and the relationship between joint positions and articular contact areas. Understanding the normal kinematics of the equine stifle and relationship between joint positions and articular contact areas may provide an important insight into the aetiology and location of common stifle joint pathologies (articular cartilage and meniscal lesions).

Authors' declaration of interests

No competing interests have been declared.

Ethical animal research

Cadaveric stifles from animals subjected to euthanasia for reasons unrelated to this study were used.

Source of funding

Supported by a Freeman Fund Grant from Michigan State University College of Veterinary Medicine, the Laboratory for Comparative Orthopaedic Research, and a NIH training grant (T35RR01749).

Acknowledgements

The authors thank Jeremy Gingrich and Nicole Hainer for technical assistance.

Authorship

S.E. Halley contributed to data analysis and interpretation. M.J. Bey contributed to study design, study execution, data analysis and interpretation. J.A. Haladik and M. Lavagnino contributed to study execution and data analysis and interpretation. S.P. Arnoczky contributed to study design, study execution, data analysis and interpretation. All authors contributed to the preparation of the manuscript and gave final approval of the manuscript.

Manufacturers' addresses

[a]EMD Technologies, Quebec, Canada.
[b]Shimadzu, Kyoto, Japan.
[c]Vision Research, Wayne, New Jersey, USA.
[d]GE Healthcare, Waukesha, Wisconsin, USA.
[e]Materialise, Leuven, Belgium.

References

1. Baxter, G.M. (1996) Subchondral cystic lesions in horses. In: *Joint Disease in the Horse*, Eds: C.W. McIlwraith and G.W. Trotter, WB Saunders, Elsevier, Philadelphia. pp 384-397.
2. Fowlie, J., Arnoczky, S., Lavagnino, M., Maerz, T. and Stick, J. (2011) Resection of grade III cranial horn tears of the equine medial meniscus alter contact forces on medial tibial condyle at full extension: an in vitro cadaveric study. *Vet. Surg.* **40**, 957-965.
3. Fowlie, J.G., Stick, J.A. and Nickels, F.A. (2012) Stifle. In: *Equine Surgery*, 4th edn., Eds: J.A. Auer and J.A. Stick, Elsevier Inc., St. Louis. pp 1419-1422.
4. Hendrix, S.M., Baxter, G.M., McIlwraith, C.W., Hendrickson, D.A., Goodrich, L.R., Frisbie, D.D. and Trotter, G.W. (2010) Concurrent or sequential development of medial meniscal and subchondral cystic lesions within the medial femorotibial joint in horses (1996-2006). *Equine Vet. J.* **42**, 5-9.
5. Walmsley, J.P. (1995) Vertical tears of the cranial horn of the meniscus and its cranial ligament in the equine femorotibial joint - 7 cases and their treatment by arthroscopic surgery. *Equine Vet. J.* **27**, 20-25.
6. Walmsley, J.P., Phillips, T.J. and Townsend, H.G. (2003) Meniscal tears in horses: an evaluation of clinical signs and arthroscopic treatment of 80 cases. *Equine Vet. J.* **35**, 402-406.
7. Walmsley, J.P. (2005) Diagnosis and treatment of ligamentous and meniscal injuries in the equine stifle. *Vet. Clin. N. Am.: Equine Pract.* **21**, 651-672.
8. Trotter, G.W. and McIlwraith, C.W. (1996) Clinical features and diagnosis of equine joint disease. In: *Joint Disease in the Horse*, Eds: C.W. McIlwraith and G.W. Trotter, WB Saunders, Elsevier, Philadelphia. pp 120-144.
9. Hurtig, M.B. and Pool, R.R. (1996) Pathogenesis of osteochondrosis. In: *Joint Disease in the Horse*, Eds: C.W. McIlwraith and G.W. Trotter, WB Saunders, Elsevier, Philadelphia. pp 335-358.
10. Taylor, W.R., Poepplau, B.M., Konig, C., Ehrig, R.M., Zachow, S., Duda, G.N. and Heller, M.O. (2011) The medial-lateral force distribution in the ovine stifle joint during walking. *J. Orthop. Res.* **4**, 567-571.
11. Arnoczky, S.P., Torzilli, P.A. and Marshall, J.L. (1977) Biomechanical evaluation of anterior cruciate ligament repair in the dog: an analysis of the instant center of motion. *J. Am. Anim. Hosp. Ass.* **13**, 553-558.
12. Frankel, V.H., Burstein, A.H. and Brooks, D.B. (1974) Biomechanics of internal derangement of the knee. Pathomechanics as determined by the instant centers of motion. *J. Bone Jt. Surg.* **53A**, 945-977.
13. Helfet, A.J. (1959) Mechanisms of derangements of the medial semilunar cartilage and their management. *J. Bone Jt. Surg.* **41B**, 319-336.
14. Luther, J.K., Cook, C.R. and Cook, J.L. (2009) Meniscal release in cruciate ligament intact stifles causes lameness and medial compartment cartilage pathology in dogs 12 weeks postoperatively. *Vet. Surg.* **38**, 520-529.
15. Rangger, C., Klestil, T., Gloetzer, W., Kemmler, G. and Benedetto, K.P. (1995) Osteoarthritis after arthroscopic partial meniscectomy. *Am. J. Sports Med.* **23**, 240-244.
16. Draganich, L.F., Andriacchi, T.P. and Andersson, G.B. (1987) Interaction between intrinsic knee mechanics and the knee extensor mechanism. *J. Orthop. Res.* **5**, 539-547.
17. Buckwalter, J.A. and Lane, N.E. (1997) Athletics and osteoarthritis. *Am. J. Sports Med.* **25**, 873-881.
18. Setton, L.A., Elliott, D.M. and Mow, V.C. (1999) Altered mechanics of cartilage with osteoarthritis: human osteoarthritis and experimental model of joint degeneration. *Osteoarth. Cartil.* **7**, 2-14.
19. Hsieh, Y.F., Draganich, L.F., Ho, S.H. and Reider, B. (2002) The effects of removal and reconstruction of the anterior cruciate ligament on the contact characteristics of the patellofemoral joint. *Am. J. Sports Med.* **30**, 121-127.
20. Tapper, J.E., Fukushima, S., Azuma, H., Thorton, G.M., Ronsky, J.L., Shrive, N.G. and Frank, C.B. (2006) Dynamic in vivo kinematics of the intact ovine stifle joint. *J. Orthop. Res.* **4**, 782-792.
21. Tashman, S., Anderst, W., Kolowich, P., Havstad, S. and Arnoczky, S. (2004) Kinematics of the ACL-deficient canine knee during gait: serial changes over two years. *J. Orthop. Res.* **22**, 931-941.
22. Fowlie, J.G., Arnoczky, S.P., Stick, J.A. and Pease, A.P. (2011) Meniscal translocation and deformation throughout the range of motion of the equine stifle joint: an in vitro cadaveric study. *Equine Vet. J.* **43**, 259-264.
23. Fredricson, I. and Drevemo, S. (1971) A new method of investigating equine locomotion. *Equine Vet. J.* **3**, 137-140.
24. Fredricson, I. (1972) *Equine Joint Kinematics and Coordination*. Thesis. Stockholm University, Stockholm.
25. Fredricson, I., Drevemo, S., Dalin, G., Hjerten, G. and Bjorne, K. (1980) The application of high-speed cinematography for the quantitative analysis of equine locomotion. *Equine Vet. J.* **12**, 54-59.
26. Crawford, W.H. and Leach, D.H. (1984) The effect of racetrack design on gait symmetry of the pacer. *Can. J. Comp. Med.* **48**, 374-380.
27. Kobluk, C.N., Schnurr, D., Horney, F.D., Sumner-Smith, G., Willoughby, R.A., Dekleer, V. and Hearn, T.C. (1989) Use of high-speed cinematography and computer generated gait diagrams for the study of equine hindlimb kinematics. *Equine Vet. J.* **21**, 48-58.
28. Hodson, E., Clayton, H.M. and Lanovaz, J.L. (2001) The hindlimb in walking horses: 1. Kinematics and ground reaction forces. *Equine Vet. J.* **33**, 38-43.
29. Back, W., Schamhardt, H.C., Savelberg, H.H., van den Bogert, A.J., Bruin, G., Hartman, W. and Barneveld, A. (1995) How the horse moves: 2. Significance of graphical representations of equine hind limb kinematics. *Equine Vet. J.* **27**, 39-45.
30. Menschik, A. (1975) Mechanik des kniegelenkes. *Z. Orthop.* **113**, 388-400.

31. Anderst, W.J. and Tashman, S. (2003) A method to estimate in vivo dynamic articular surface interaction. *J. Biomech.* **36**, 1291-1299.
32. Tashman, S., Collon, D., Anderson, K., Kolowich, P. and Anderst, W. (2004) Abnormal rotational knee motion during running after anterior cruciate ligament reconstruction. *Am. J. Sports Med.* **32**, 975-983.
33. Bey, M.J., Kline, S.K., Zauel, R., Kolowich, P.A. and Lock, T.R. (2010) In vivo measurement of glenohumeral joint contact patterns. *EURASIP J. Adv. Signal Process.* **2010**, Article No. 5.
34. Anderst, W., Zauel, R., Bishop, J., Demps, E. and Tashman, S. (2009) Validation of three-dimensional model-based tibio-femoral tracking during running. *Med. Eng. Phys.* **31**, 10-16.
35. Goyal, K., Tashman, S., Wang, J.H., Li, K., Zhang, X. and Harner, C. (2012) *In vivo* analysis of the isolated posterior cruciate ligament-deficient knee during functional activities. *Am. J. Sports Med.* **40**, 777-785.
36. Anderst, W.J., Les, C. and Tashman, S. (2005) *In vivo* serial joint space measurements during dynamic loading in a canine model of osteoarthritis. *Osteoarth. Cartil.***13**, 808-816.
37. Tashman, S. and Anderst, W. (2003) *In-vivo* measurement of dynamic joint motion using high speed biplane radiography and CT: application to canine ACL deficiency. *J. Biomech. Eng.* **125**, 238-245.
38. Deneweth, J.M., Bey, M.J., McLean, S.G., Lock, T.R., Kolowich, P.A. and Tashman, S. (2010) Tibiofemoral joint kinematics of the anterior cruciate ligament-reconstructed knee during a single-legged hop landing. *Am. J. Sports Med.* **38**, 1820-1828.
39. Tashman, S., Kolowich, P., Collon, D., Anderson, K. and Anderst, W. (2007) Dynamic function of the ACL-reconstructed knee during running. *Clin. Orthop. Rel. Res.* **454**, 66-73.
40. Frisbie, D.D., Cross, M.W. and McIlwraith, C.W. (2006) A comparative study of articular cartilage thickness in the stifle of animal species used in human pre-clinical studies compared to articular cartilage thickness in the human knee. *Vet. Comp. Orthop. Traumatol.* **3**, 142-146.
41. Blankevoort, L., Huiskes, R. and de Lange, A. (1988) The envelope of passive knee joint motion. *J. Biomech.* **21**, 705-720.
42. Lafortune, M.A., Cavanagh, P.R., Sommer, H.J. III and Kalenak, A. (1992) Three-dimensional kinematics of the human knee during walking. *J. Biomech.* **25**, 347-357.
43. Kenawey, M., Liodakis, E., Krettek, C., Ostermeiser, S., Horn, T. and Hankemeiser, S. (2011) Effect of the lower limb rotational alignment on tibiofemoral contact pressure. *Knee Surg. Sports Traumatol. Arthrosc.* **19**, 1851-1859.
44. Senter, C. and Hame, S.L. (2006) Biomechanical analysis of tibial torque and knee flexion angle: implications for understanding knee injury. *Sports Med.* **36**, 635-641.
45. Englund, M. (2010) The role of biomechanics in the initiation and progression of OA of the knee. *Best Pract. Res. Clin. Rheumatol.* **24**, 39-46.
46. Andriacchi, T.P., Briant, P.L., Bevill, S.L. and Koo, S. (2006) Rotational changes at the knee after ACL injury cause cartilage thinning. *Clin. Orthop. Rel. Res.* **442**, 39-44.
47. Suganuma, J. and Ohkoshi, T. (2011) Association of internal rotation of the knee joint with recurrent subluxation of the lateral meniscus. *Arthroscopy* **8**, 1071-1078.
48. Kawashima, K., Tomita, T., Tamaki, M., Murase, T., Yoshikawa, H. and Sugamoto, K. (2013) In vivo three-dimensional motion analysis of osteoarthritic knees. *Mod. Rheumatol.* **23**, 646-652.
49. Müller, W. (1983) *The Knee: Form, Function, and Ligament Reconstruction*, W. Müller, Springer-Verlag, Bermin, New York. pp 8-60.
50. Torres, B.T., Punke, J.P., Fu, Y.-C., Navik, J.A., Speas, A.L., Sornborger, A. and Budsberg, S.C. (2010) Comparison of canine stifle kinematic data collected with three different targeting models. *Vet. Surg.* **39**, 504-512.
51. O'Connor, J.J., Shercliff, T., Fitzpatrick, D., Bradley, J., Daniel, D. and Biden, E. (1990) Geometry of the knee. In: *Knee Ligaments: Structure. Function, Injury, and Repair*, Eds: D. Daniels, W. Akeson and J. O'Connor, Raven Press, New York. pp 163-199.
52. Vasseur, P.B. and Arnoczky, S.P. (1981) Collateral ligaments of the canine stifle joint: anatomic and functional analysis. *Am. J. Vet. Res.* **42**, 1133-1137.
53. Changoor, A., Hurtig, M.B., Runciman, R.J., Quesnel, A.J., Dickey, J.P. and Lowerison, M. (2006) Mapping of donor and recipient site properties for osteochondral graft reconstruction of subchondral cystic lesions in the equine stifle joint. *Equine Vet. J.* **38**, 330-336.
54. Petersen, M.M., Olsen, C., Lauritzen, J.B., Lund, B. and Hede, A. (1996) Late changes in bone mineral density of the proximal tibia following total or partial medial meniscectomy: a randomized study. *J. Orthop. Res.* **14**, 16-21.
55. Victor, J., Labey, L., Wong, P., Innocenti, B. and Belleman, J. (2010) The influence of muscle load on tibiofemoral knee kinematics. *J. Orthop. Res.* **28**, 419-428.